NANO LETTERS

LETTER

pubs.acs.org/NanoLett

Subcellular Resolution Mapping of Endogenous Cytokine Secretion by Nano-Plasmonic-Resonator Sensor Array

Sheng Wang,[†] Sadao Ota,[†] Bin Guo,[†] Jongeun Ryu,[‡] Christopher Rhodes,[†] Yi Xiong,[†] Sheraz Kalim,[§] Li Zeng,[†] Yong Chen,[‡] Michael A. Teitell,[§] and Xiang Zhang*[,†,∥]

[†]NSF Nanoscale Science and Engineering Center (NSEC), 3112 Etcheverry Hall, University of California, Berkeley, California 94720, United States

[‡]Department of Mechanical and Aerospace Engineering, University of California, Los Angeles, California 90095, United States

[§]Department of Pathology and Laboratory Medicine, University of California, Los Angeles, California 90095, United States

[∥]Materials Sciences Division, Lawrence Berkeley National Laboratory, 1 Cyclotron Road, Berkeley, California 94720, United States

Supporting Information

ABSTRACT: Local extracellular signaling is central for cellular interactions and organizations. We report a novel sensing technique to interrogate extracellular signaling at the subcellular level. We developed an in situ immunoassay based on giant optical enhancement of a tunable nano-plasmonic-resonator array fabricated by nanoimprint lithography. Our nanoplasmonic device significantly increases the signal-to-noise ratio to enable the first time submicrometer resolution quantitative mapping of endogenous cytokine secretion. Our study shows a markedly high local interleukin-2 (IL-2) concentration within the immediate vicinity of the cell which finally validates a decades-old hypothesis on autocrine physiological concentration and spatial range. This general sensing technique can be applied for a broad range of cellular communication studies to improve our understanding of subcellular signaling and function.

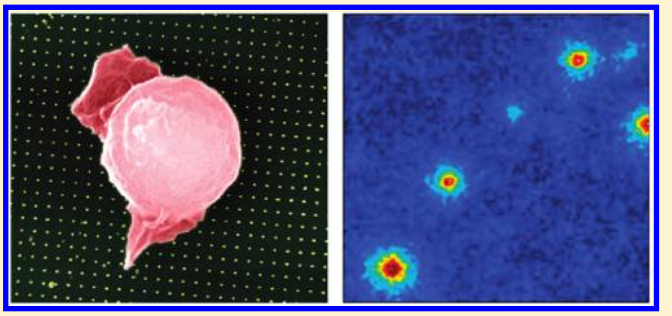

KEYWORDS: Biosensing, plasmonic resonator, in situ immunoassay, cytokine, T cell, nanoimprint lithography (NIL)

Extracellular signaling controls how cells communicate, differentiate, and organize to form unique biological systems with extraordinary physiological functions. Signaling molecules transfer information not only via their chemical compositions but also through their spatiotemporal distributions. Cells could confine intended information within a local area by controlling the spatial profile of signaling molecules or through regulated spatial variations in target cell response thresholds. Therefore, to decode cellular communications at the subcellular level, a high spatial resolution signaling molecule sensing platform is required. For instance, autocrine signaling, which regulates a cell through self-secreted factors feeding back on that cell, requires spatiotemporal control over secreted signaling molecules to regulate local essential physiological and pathological processes.[1−4] For example, an interleukin-2 (IL-2) autocrine loop is essential for T lymphocyte expansions and also related to cancerogenesis.[1,3,4] While our understanding of autocrine processes is limited by traditional biosensing techniques,[5] it has been hypothesized that autocrine loops should be highly localized processes, suggesting unproven spatial constraints on cellular secretions to regulate autocrine signaling responses.[5−7] Theoretical analyses[5,6] and indirect evidence obtained by microphysiometer and ligand-binding assays[7] predict that the physiologically effective local concentration of cytokines in the proximity of target cells should be several orders of magnitude higher than the global concentrations measured in the serum. However, direct quantification has thus far not been possible due to the limitations of current biosensing techniques to probe spatially confined signaling processes.[5]

Nanosensing techniques offer new opportunities for in situ high-resolution extracellular sensing,[8] for example, a redox signaling molecule H_2O_2 can be mapped in subcellular resolution with carbon nanotube array sensors.[9] Modern molecular and cellular biology research calls for a general nanosensing tool for many kinds of extracellular signaling molecules detection with subcelluar resolution. Plasmonic nanostructures provide a novel approach to concentrating electromagnetic energy at the nanoscale, and they can significantly enhance biosensing signals, such as for surface enhanced raman scattering (SERS) measurements.[10] Many novel nanostructures have been explored for ultrasensitive biosensor applications[11−15] with one powerful structure being a tunable nanoplasmonic resonator (TNPR).[16,17] TNPRs are multilayered nanoplasmonic structures that consist of feature sizes in the range of 100 nm that are assembled from alternating noble metal and dielectric films.[16,17] TNPRs provide unique advantages, such as extraordinary field enhancements, tunable resonance frequencies, and compatibility with a top-down

Received: June 2, 2011
Revised: July 21, 2011
Published: July 22, 2011

mass production process which enables the fabrication of large numbers of uniform nanoplasmonic structures with controllable resonance spectra and electromagnetic field enhancements. Plasmon-enhanced fluorescence is regarded as an emerging tool in biosensing,[18,19] while it has not yet been fully explored in biosensing applications due to contrasting effects on signal enhancement and quenching.[20,21] Mechanistic studies have shown that in order to achieve maximal fluorescence enhancement there is an optimized range of distances between a fluorophore and the device metal surface which, fortunately, falls within the length scale of antibody−antigen−antibody sandwich structures, such as those used in fluorescent immunoassay.[20] Furthermore, a large number of uniform biosensing nanostructures can be fabricated by nanoimprint lithography (NIL).[22,23] The NIL mass fabrication method produces high-quality TNPRs at a low cost, which potentially offers a unique opportunity for high-resolution mapping of signaling molecule secretion. Thus, the combination of NIL[22,23] for large scale TNPR fabrication and the theoretical ability for TNPR enhancement of in situ immunoassays suggests a possible method to significantly enhance a fluorescent detection signal along with markedly improving the signal-to-noise ratio for accurate biosensing. The signal amplification of the conventional enzyme-linked immunosorbent assay (ELISA) relies on the catalyzation of the enzyme; the diffusive nature of the reporter molecules limits its applications in high-resolution sensing. Conventional fluorescent immunoassay is based on spatial integration of individual signals. Due to the weak signal strength, the signal-to-noise ratio drops drastically in subcellular scale. On the other hand, the averaging of the signals over larger area scarifies the spatial resolution and hampers its ability to sense the local extracellular secretion. There were efforts in signaling molecule sensing at the single cell level attempting to overcome this significant limitation.[24−26] However, in situ biosensing techniques, such as elispot,[25] cannot achieve subcellular spatial resolution because of poor signal-to-noise ratios or blurry staining from diffusive reporters at the subcellular scale. The significant optical enhancement of TNPRs is crucial to remove the requirement for the large area spatial integration thus making it possible for subcellular resolution biosensing. Here, we report a novel technique, termed a TNPR-enhanced in situ immunoassay, which we successfully demonstrate quantifies and maps endogenous cytokine secretion from individual cells at subcellular resolution. Our study is the first direct quantification that confirms the theoretical decades-old hypothesis[6] that IL-2, which can function as an autocrine signaling molecule, has a significantly elevated local target cell concentration.

The experimental platform for the TNPR-enhanced in situ immunoassay for subcellular resolution mapping of cytokine secretion is shown schematically in Figure 1. A TNPR array 100 nm in diameter with a 500 nm periodicity was fabricated by NIL (Supplementary Figure S1, Supporting Information) and was coated with poly-D-lysine and an anti-IL-2 antibody. Jurkat T cells were cultured on the anti-IL-2 functionalized TNPR surface, imaged by scanning electron microscopy (SEM, Figure 1 inset) to verify cell orientation on the array, and followed by costimulation with a phorbol ester, phorbol myristal acetate (PMA), and a calcium ionophore, ionomycin. A portion of the large amount of IL-2 secreted by Jurkat T cells using this activation method[27] was captured by IL-2 antibodies immobilized on the device surface. This was followed by the addition of a fluorescence-conjugated anti-IL-2 antibody to detect the captured IL-2 on the TNPR surface. Formation of the antibody−antigen−antibody sandwich

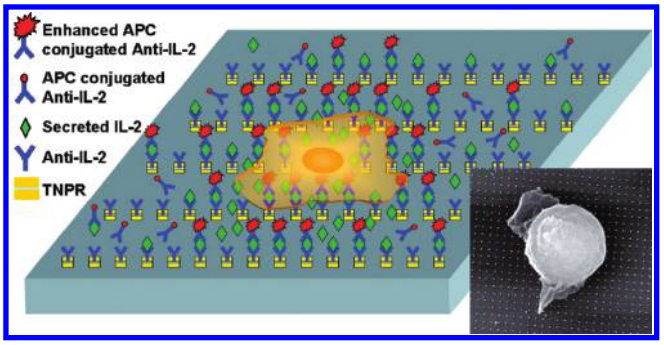

Figure 1. Schematic of high-resolution mapping of cytokine secretion by a TNPR-enhanced in situ immunoassay. A TNPR array fabricated by NIL was incubated with anti-IL-2 antibody, and after Jurkat T cell plating, stimulation, and removal, a portion of the secreted IL-2 was captured by the antibodies on TNPR. Fluorescence-conjugated antibodies were applied to detect the secreted IL-2 by forming an antibody−antigen (IL-2)−antibody sandwich on the TNPR surface. Insert: SEM image of a Jurkat T cell adherent to a TNPR array (500 nm pitch).

complex brings the fluorophore into the optimal distance for TNPR-dependent signal enhancement. Nonspecifically bound fluorescence-conjugated antibody will be too close to the TNPR surface and therefore experience less signal enhancement due to a dominant quenching effect. Also, there will be no signal enhancement when nonspecific binding occurs in the empty areas of the device surface between TNPRs. Therefore, the anticipated signal-to-noise ratio should be strongly improved as the TNPRs will specifically enhance signal detection from antibody−antigen−antibody sandwich complexes over nonspecific binding interactions. Following a thorough rinse to remove the Jurkat T cells, the profile of secreted IL-2 will be mapped at submicrometer resolution because of the enhanced signal strength and improved signal-to-noise ratio.

Numeric analysis and characterization of the TNPR-enhanced IL-2 immunoassay were performed. As we reported previously,[16,17] the TNPR structure is 100 nm in diameter and consists of two 20 nm gold layers with an intervening 5 nm silicon dioxide thin film (Figure 2a). The TNPR extinction spectrum shows that the resonance peak is ∼670 nm (Figure 2a) with the strongest electric field enhancement located close to the TNPR edge around the polarization direction of the incident light (Figure 2b). The light intensity enhancement factor reached 2 to 3 orders of magnitude at this edge (Figure 2b). Because optimized fluorescence enhancement occurs at ∼10 nm from a gold surface,[20,21] the TNPR functions robustly in an IL-2 sandwich immunoassay based upon the proximal geometry of this antibody−antigen−antibody complex. Notably, there is still significant field enhancement 10 nm away from the gold TNPR surface (Figure 2b). Spectrum matching is also essential for plasmon-enhanced fluorescence. Thus, we chose APC (allophycocyanin) conjugated anti-IL-2 as the detection antibody, which has a matched overlap spectrum with the designed TNPR. To determine the extent of TNPR enhancement, we assessed a purified IL-2 solution without cells using an APC conjugated anti-IL-2 antibody for detection (Figure 2c). These clearly resolved individual TNPRs in the fluorescent image (Figure 2c) were not only indicating the enhancement but also showing the submicrometer spatial resolution as high as 500 nm of the pitch size. The normalized fluorescence signal was enhanced 117-fold in the TNPR area versus the area of the platform that lacked TNPRs. Factors contributing

dx.doi.org/10.1021/nl2018838 |*Nano Lett.* 2011, 11, 3431–3434

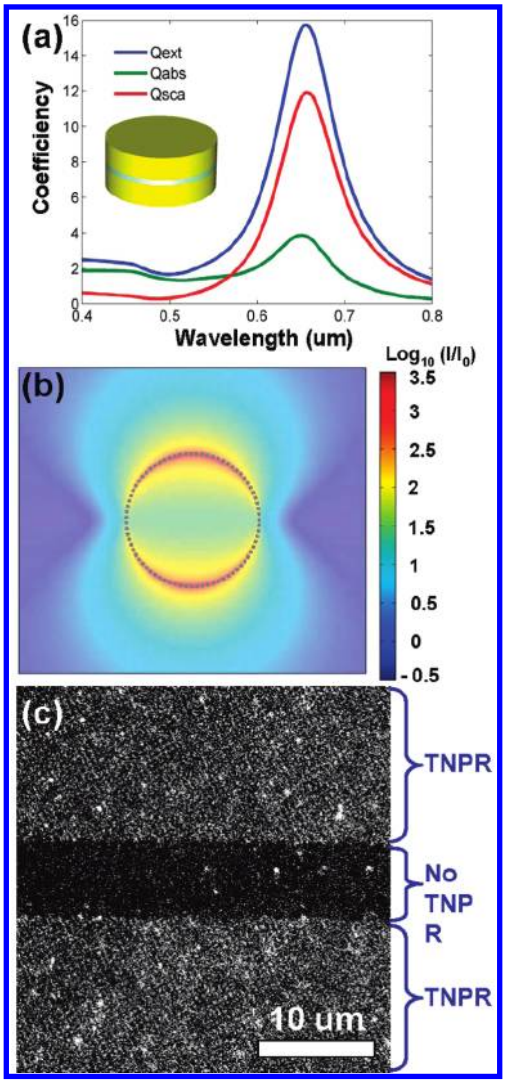

Figure 2. Physical principle, simulation, and experimental validation of the TNPR-enhanced immunoassay. (a) Simulation results of TNPR plasmonic resonance spectrum (blue, green, and red curves represent extinction, absorption, and scattering, respectively). (b) Spatial distribution of the optical intensity enhancement at the plane above the top surface of a TNPR (100 nm diameter). (c) Fluorescent image showing experimental validation of the TNPR-enhanced immunoassay, with a fluorescence enhancement factor of ~117.

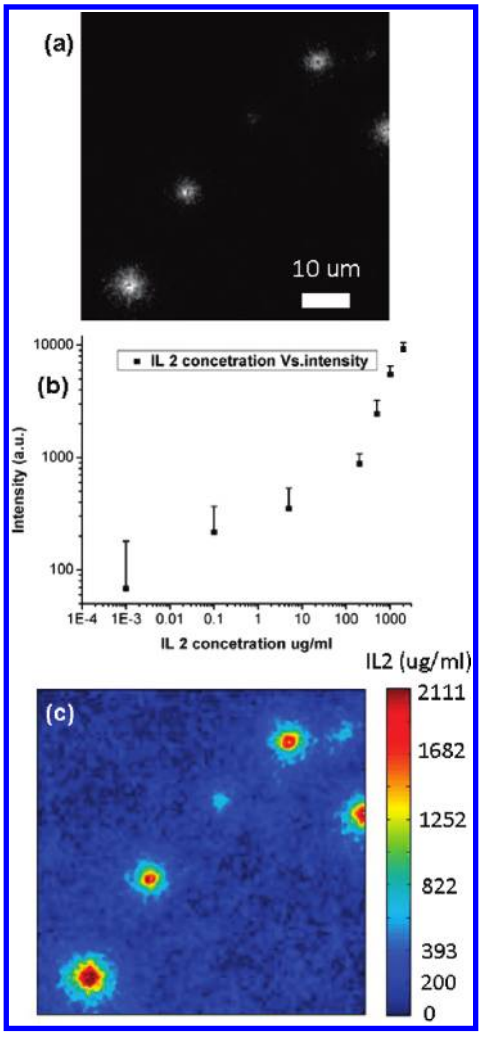

Figure 3. Demonstration of quantitative high spatial resolution mapping of IL-2 secretion from individual Jurkat T cells. (a) Individual Jurkat T cells IL-2 secretion patterns. (b) Calibration curve for increasing concentrations of IL-2 detected with optical signal intensity. (c) Quantitative mapping of Jurkat T cell secretion profiles using information gathered in panels a and b.

to signal enhancement and noise reduction include the local plasmon field and the gold TNPR surface, which has a higher affinity for antibody binding.

Next, a cytokine secretion experiment was performed. Jurkat T cells were cultured on top of an anti-IL-2 antibody-functionalized TNPR array. After overnight stimulation, APC conjugated anti-IL-2 antibody was added followed by washing to remove the cells and unbound antibody. A high-resolution map of the IL-2 secretion profile from individual Jurkat T cells was generated (Figure 3a). Results showed the highest concentration of IL-2 in the immediate vicinity of the cell, close to the center of the profile pattern from each cell, which also produced a fast signal decay moving radially from this region into a low signal intensity background. As the Jurkat T cells were nonpolarized, it was not surprising that the secretion pattern was round and symmetrically decayed into the background. Control experiments showed that stimulation with PMA and ionomycin was necessary to induce IL-2 secretion (Supplementary Figure S2, Supporting Information) and that the enhancement from TNPR was essential to achieving enough sensitivity for high resolution sensing this secretion (Supplementary Figure S3, Supporting Information). The secretion data were quantified using an IL-2 calibration curve (Figure 3b). Our results (Figure 3c) showed that the local concentration of IL-2 at the cell membrane was on the order of hundreds of μg/mL to mg/mL which fell into the right range covered by the calibration curve. By contrast, for a cell density of 10^6 cells/mL after stimulation the global IL-2 concentration was the in the ng/mL range.

Previous studies hypothesize that the concentration of IL-2 reduces significantly with distance from a cell[5−7] due to diffusion, which suggests that the local IL-2 concentration would be much higher than that measured globally. Indeed, the concentration we measured locally compared to that in the medium was ~5 to 6 orders of magnitude different. Since the IL-2 concentration in presecretion vesicles is estimated to be tens of mg/mL[6] and

dx.doi.org/10.1021/nl2018838 |*Nano Lett.* 2011, 11, 3431–3434

diffusion at the nanoscale is very fast (<1 ms), it is not immediately clear why the time-averaged IL-2 concentration near the cell membrane could reach hundreds of μg/mL to mg/mL. As shown before[6,27] both the IL-2 and the α-chain of the IL-2 receptor were largely produced within the same cell after stimulation. As the IL-2 was secreted, the α chain of IL-2 receptor combined with the β and γ chain complex to form high affinity IL-2 receptors (K_d = 10 pM) on the cell membrane. A portion of the secreted IL-2 binds to those receptors, which may prevent the rapid escape of IL-2 and maintain the high average IL-2 concentration near the cell membrane.[6] A competing factor that could reduce this high local IL-2 concentration would be receptor-mediated endocytosis, but from our measurements this seems to be ineffective at reducing the IL-2 content in the immediate cell vicinity. This spatiotemporal IL-2 secretion profile may have important roles in such extracellular signaling.[5−7,28]

The TNPR technique demonstrated in this report can quantify subcellular cytokine secretion. An important future application is to determine the signaling molecule spatial distribution between polarized cells, such as those during the signaling and communication events between neuronal or immunological synapses.[29,30] This TNPR technique will also enable the simultaneous detection, spatial mapping, and quantification of multiple, distinct signaling molecules when TNPRs are engineered with multiple resonance peaks for multiple color enhancements. Our technique opens a new avenue in sensing and quantifying subcellular level signaling molecule secretion and could have broad impact for deciphering extracellular signaling and function.

■ ASSOCIATED CONTENT

Supporting Information. Experimental details and supplementary figures showing TNPR fabrication and SEM imaging, TNPR-enhanced in situ immunoassay showing that cell stimulation was required for IL-2 secretion, and enhancement from TNPRs was essential for mapping and quantifying IL-2 secretion. This material is available free of charge via the Internet at http://pubs.acs.org.

■ AUTHOR INFORMATION

Corresponding Author
*E-mail: xiang@berkeley.edu.

■ ACKNOWLEDGMENT

We thank Dr. Ajithkumar Warrier for the helpful discussions. The authors acknowledge National Institutes of Health (NIH) funding through the Nanomedicine Development Center (Center for Cell Control, PN2EY018228), an NIH Roadmap award. This work was also supported in part by National Science Foundation (NSF) Nanoscale Science and Engineering Center (SINAM; CMMI-0751621).

■ REFERENCES

(1) Toribio, M. L.; Gutierrez-Ramos, J. C.; Pezzi, L.; Marcos, M. A. R.; Martinez-A, C. *Nature* **1989**, *342*, 82–85.
(2) Nurieva, R.; Yang, X. O.; Martinez, G.; Zhang, Y.; Panopoulos, A. D.; Ma, L.; Schluns, K.; Tian, Q.; Watowich, S. S.; Jetten, A. M.; Dong, C. *Nature* **2007**, *448*, 480–483.
(3) Sporn, M. B.; Roberts, A. B. *Nature* **1985**, *313*, 745–747.
(4) Arima, N.; Daitoku, Y.; Ohgaki, S.; Fukumori, J.; Tanaka, H.; Yamamoto, Y.; Fujimoto, K.; Onoue, K. *Blood* **1986**, *68*, 779–782.
(5) Shvartsman, S. Y.; Wiley, H. S.; Deen, W. M.; Lauffenburger, D. A. *Biophys. J.* **2001**, *81*, 1854–1867.
(6) Kaplan, D. *Immunol. Today* **1996**, *17*, 303–304.
(7) Lauffenburger, D. A.; Oehrtman, G. T.; Walker, L.; Wiley, H. S. *Proc. Natl. Acad. Sci. U.S.A.* **1998**, *95*, 15368–15373.
(8) Sokolov, A. N.; Roberts, M. E.; Bao, Z. *Mater. Today* **2009**, *12*, 12–20.
(9) Jin, H.; Heller, D. A.; Kalbacova, M.; Kim, J.-H.; Zhang, J.; Boghossian, A. A.; Maheshri, N.; Strano, M. S. *Nat. Nanotechnol.* **2010**, *5*, 302–309.
(10) Nie, S.; Emory, S. R. *Science* **1997**, *275*, 1102–1106.
(11) Prokes, S. M.; Glembocki, O. J.; Rendell, R. W.; Ancona, M. G. *Appl. Phys. Lett.* **2007**, *90*, 093105.
(12) Stewart, M. E.; Anderton, C. R.; Thompson, L. B.; Maria, J.; Gray, S. K.; Rogers, J. A.; Nuzzo, R. G. *Chem. Rev* **2008**, *108*, 494–521.
(13) Wang, S.; Pile, D. F. P.; Sun, C.; Zhang, X. *Nano Lett.* **2007**, *7*, 1076–1080.
(14) Anker, J. N.; Hall, W. P.; Lyandres, O.; Shah, N. C.; Zhao, J.; Van Duyne, R. P. *Nat. Mater.* **2008**, *7*, 442–453.
(15) Kabashin, A. V.; Evans, P.; Pastkovsky, S.; Hendren, W.; Wurtz, G. A.; Atkinson, R.; Pollard, R.; Podolskiy, V. A.; Zayats, A. V. *Nat. Mater.* **2009**, *8*, 867–871.
(16) Su, K. H.; Wei, Q. H.; Zhang, X. *Appl. Phys. Lett.* **2006**, *88*, 063118.
(17) Sun, C.; Su, K.-H.; Valentine, J.; Rosa-Bauza, Y. T.; Ellman, J. A.; Elboudwarej, O.; Mukherjee, B.; Craik, C. S.; Shuman, M. A.; Chen, F. F.; Zhang, X. *ACS Nano* **2010**, *4*, 978–984.
(18) Aslan, K.; Gryczynski, I.; Malicka, J.; Matveeva, E.; Lakowicz, J. R.; Geddes, C. D. *Curr. Opin. Biotechnol.* **2005**, *16*, 55–62.
(19) Pompa, P. P.; Martiradonna, L.; Torre, A. D.; Sala, F. D.; Manna, L.; De Vittorio, M.; Calabi, F.; Cingolani, R.; Rinaldi, R. *Nat. Nanotechnol.* **2006**, *1*, 126–130.
(20) Anger, P.; Bharadwaj, P.; Novotny, L. *Phys. Rev. Lett.* **2006**, *96*, 113002.
(21) Kinkhabwala, A.; Yu, Z.; Fan, S.; Avlasevich, Y.; Mullen, K.; Moerner, W. E. *Nat. Photonics* **2009**, *3*, 654–657.
(22) Chou, S. Y.; Krauss, P. R.; Renstrom, P. J. *Science* **1996**, *272*, 85–87.
(23) Stuart, C.; Xu, Q.; Tseng, R. J.; Yang, Y.; Hahn, H. T.; Chen, Y.; Wu, W.; Williams, R. S. *J. Vac. Sci. Technol., B* **2006**, *24*, 539.
(24) Yee, C.; Greenberg, P. *Nat. Rev. Cancer* **2002**, *2*, 409–419.
(25) Lakew, M.; Nordström, I.; Czerkinsky, C.; Quiding-Järbrink, M. *J. Immunol. Methods* **1997**, *203*, 193–198.
(26) Qian, W. J.; Aspinwall, C. A.; Battiste, M. A.; Kennedy, R. T. *Anal. Chem.* **2000**, *72*, 711–717.
(27) Abraham, R. T.; Weiss, A. *Nat. Rev. Immunol.* **2004**, *4*, 301–308.
(28) Andersson, J.; Abrams, J.; Björk, L.; Funa, K.; Litton, M.; Agren, K.; Andersson, U. *Immunology* **1994**, *83*, 16–24.
(29) Howe, C. L.; Mobley, W. C. *Curr. Opin. Neurobiol.* **2005**, *15*, 40–48.
(30) Fooksman, D. R.; Vardhana, S.; Vasiliver-Shamis, G.; Liese, J.; Blair, D.; Waite, J.; Sacristán, C.; Victora, G.; Zanin-Zhorov, A.; Dustin, M. L. *Annu. Rev. Immunol.* **2010**, *28*, 79–105.